CrossMark

J. Fluid Mech. (2016), *vol.* 803, *pp.* 516–527. © Cambridge University Press 2016
doi:10.1017/jfm.2016.496

Maximum drop radius and critical Weber number for splashing in the dynamical Leidenfrost regime

Guillaume Riboux[1,†] **and José Manuel Gordillo**[1]

[1]Área de Mecánica de Fluidos, Departamento de Ingeniería Aeroespacial y Mecánica de Fluidos, Universidad de Sevilla, Avenida de los Descubrimientos s/n 41092, Sevilla, Spain

(Received 17 March 2016; revised 14 June 2016; accepted 21 July 2016; first published online 30 August 2016)

At room temperature, when a drop impacts against a smooth solid surface at a velocity above the so-called critical velocity for splashing, the drop loses its integrity and fragments into tiny droplets violently ejected radially outwards. Below this critical velocity, the drop simply spreads over the substrate. Splashing is also reported to occur for solid substrate temperatures above the Leidenfrost temperature, T_L, for which a vapour layer prevents the drop from touching the solid. In this case, the splashing morphology differs from the one reported at room temperature because, thanks to the presence of the gas layer, the shear stresses acting on the liquid can be neglected. Our purpose here is to predict, for wall temperatures above T_L, the critical Weber number for splashing as well as the maximum spreading radius. First, making use of boundary integral simulations, we calculate both the time evolution of the liquid velocity as well as the height of the sheet which is ejected tangentially to the substrate. These results are then used as boundary conditions for the one-dimensional mass and momentum equations describing the dynamics of the rim limiting the expanding liquid sheet. Our predictions for both the maximum spreading radius and for the critical Weber number for splashing are in good agreement with experimental observations.

Key words: breakup/coalescence, drops and bubbles, drops

1. Introduction

The understanding of the spreading or the breakup processes of a drop impacting onto a solid substrate is an area of current active research because of its relevance in a number of technological applications such as coating, cleaning, cooling and combustion (Josserand & Thoroddsen 2016). It is known that, at room temperature, drop splashing not only depends on the radius R, the impacting velocity V, the density ρ, the viscosity μ and the interfacial tension σ of the liquid, but also on the material properties of the gas, on the gas pressure (Xu, Zhang & Nagel 2005) and on the physicochemical properties of the substrate (Duez *et al.* 2007). For the case of drops impacting a smooth and dry solid substrate at room temperature, illustrated in figure 1, it can be observed that once the drop touches the solid at $T = 0$, a small

†Email address for correspondence: griboux@us.es

https://doi.org/10.1017/jfm.2016.496 Published online by Cambridge University Press

bubble – which has no influence on the subsequent dynamics – is entrapped near the axis of symmetry. Subsequently, at the ejection time T_e, a thin sheet of liquid is expelled from the radial position $A(T_e)$, with $\pi A^2(T_e)$ the area of the wetted region. Then, if the impact velocity is below the critical velocity for splashing, $V < V^*$, the ejected lamella spreads tangentially along the solid; however, if $V > V^*$, the edge of the liquid sheet dewets the solid as a consequence of the lift forces exerted by the surrounding gas (see Riboux & Gordillo (2014), hereafter RG14). Then, capillary and Rayleigh–Taylor disturbances grow in the azimuthal direction of the rim, causing its disintegration into drops. At room temperature, splashing will occur only if the liquid front is able to dewet the solid. However, when the temperature of the substrate is above T_L, with T_L the Leidenfrost temperature, the liquid never touches the substrate, independent of the value of the impact velocity because under these conditions, the drop levitates on its own vapour (Shirota *et al.* 2016). Consequently, the critical velocity for splashing will strongly depend on whether the solid temperature is below or above T_L, as it has been recently reported by Staat *et al.* (2015). In addition, as a consequence of the frictionless motion of the liquid with the substrate, the maximum spreading diameter of impacting drops increases for temperatures above T_L with respect to the case of drop impact at room temperature (Lastakowski *et al.* 2014; Wilderman *et al.* 2016).

In this contribution we aim to predict, for temperatures of the substrate above T_L, the maximum spreading radius of the drop as well as the critical impact velocity above which the drop disintegrates into smaller droplets. Moreover, for impact velocities larger than the critical one, we will also provide results for the velocities and for the diameters of the tiny droplets ejected. For this purpose, the flow field within the ejected lamella is modelled using a ballistic approximation and next, making use of integral balances of mass and momentum, the dynamics of the rim is described. A similar study was carried out by Riboux & Gordillo (2015) (from now on RG15), where the analytical expressions for the liquid velocity and the height of the liquid sheet deduced in RG14 were used as boundary conditions for the equations describing the flow in the expanding lamella. One of our main contributions here is that these analytical expressions are substituted by universal time-dependent functions calculated numerically using a boundary integral method (BIM). We find that, for short times after impact, the simulations are in excellent agreement with the theoretical predictions in RG14 but, for times $T \sim R/V$, these numerical results depart from those in RG14 and also from the equations provided in Roisman (2009), Eggers *et al.* (2010). The differences found are essential to correctly predict the experiments.

Potential flow numerical simulations will be carried out using the BIM described in Rodríguez-Rodríguez, Gordillo & Martínez–Bazán (2006), Gordillo & Gekle (2010). This type of code is adequate to simulate the splashing of drops for substrate temperatures above T_L since: (i) the vorticity in the falling drop is initially zero and (ii) the shear stresses acting in the circular region of radius $A(T)$ below the drop – see figure 1 – are negligible because, in the dynamic Leidenfrost regime, a thin vapour layer prevents the liquid from touching the wall. Therefore, the production of vorticity is restricted to regions near the free surface where the interfacial curvature is highest, e.g. the region where the impacting drop meets the ejected liquid sheet. Consequently, the flow field after the impact is mostly irrotational except in very narrow regions localized near the free surface. Motivated by this fact, in this contribution, we approximate the velocity field within the drop as $\boldsymbol{v} = \nabla\Phi$, with Φ the velocity potential satisfying the impenetrability condition at $Z = 0$, $\partial\Phi/\partial Z = 0$. In addition, thanks to the symmetry of the flow with respect to the plane $Z = 0$, $\boldsymbol{v}$ is

https://doi.org/10.1017/jfm.2016.496 Published online by Cambridge University Press

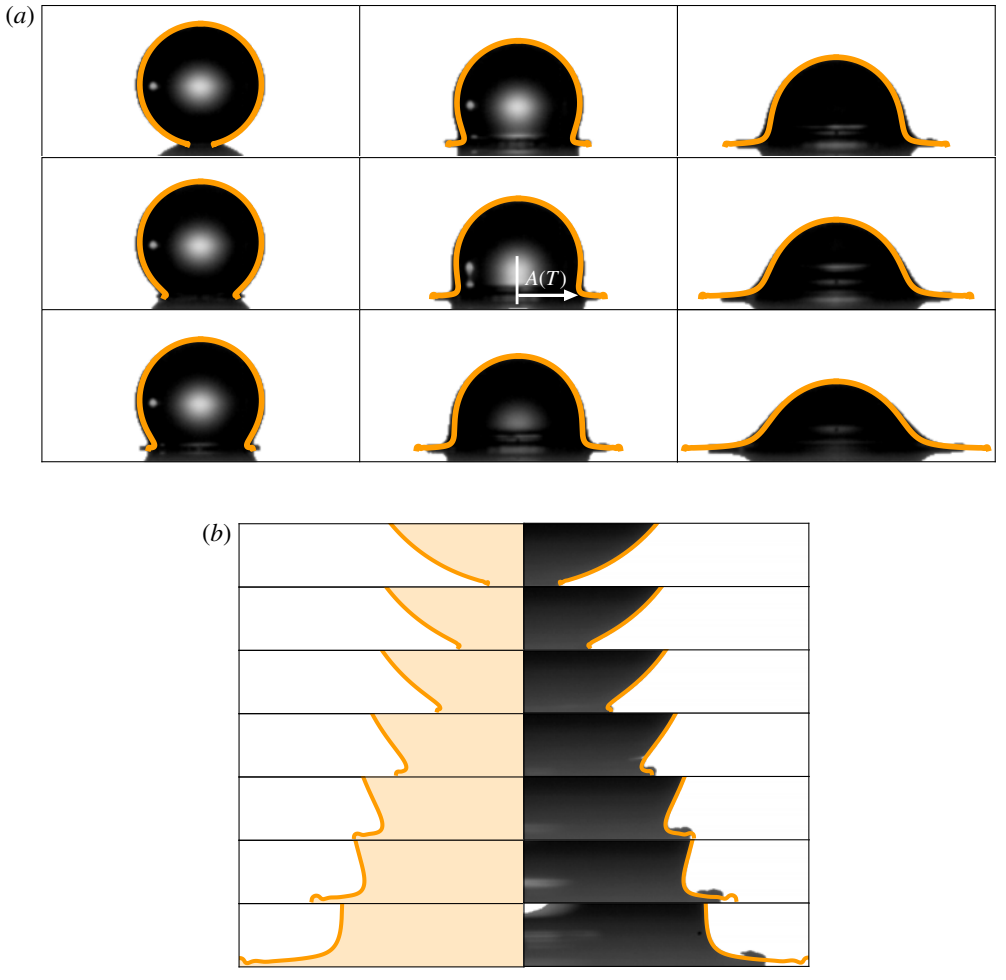


FIGURE 1. (Colour online) (*a*) The sequence of images illustrate an ethanol drop of initial radius $R = 1.03$ mm impacting against a dry smooth solid surface at room temperature with a velocity $V = 1.69$ m s^{-1} – $We = \rho V^2 R/\sigma = 100$ and $Re = \rho VR/\mu = 1360$ – at times $t \simeq 0$, $t = 0.10$, $t = 0.19$, $t = 0.29$, $t = 0.38$, $t = 0.48$, $t = 0.57$, $t = 0.76$, $t = 0.95$ with $t = TV/R$. The bright line represents the result of the boundary integral simulation, which is carried out using a number of nodes N that increases dynamically in time ($N(T = 0) = 501$). Nodes are clustered in the regions with the highest curvature. The radius of the wetted area $A(T)/R = a(t) = \sqrt{3t}$ (Riboux & Gordillo 2014) is indicated. (*b*) The right column is a zoom in of the region where the lamella is ejected for different instants of time, namely, $t = 0.016$, 0.049, 0.082, 0.164, 0.246, 0.328 and 0.491. For reference, the left column illustrates the numerical results for the same values of t. The absence of viscous shear stresses causes the rim to flow faster in the numerical simulations than in the experiments.

calculated here as the result of the head on collision of two drops of identical radii R moving with respective velocities $V\boldsymbol{e}_z$ and $-V\boldsymbol{e}_z$. Here, $\boldsymbol{e}_z$ indicates the unit vector pointing in the opposite direction to that of the falling drop. The comparison of the experimental images corresponding to an ethanol drop impacting a solid substrate at room temperature with the numerical profiles is provided in figure 1. Except

https://doi.org/10.1017/jfm.2016.496 Published online by Cambridge University Press

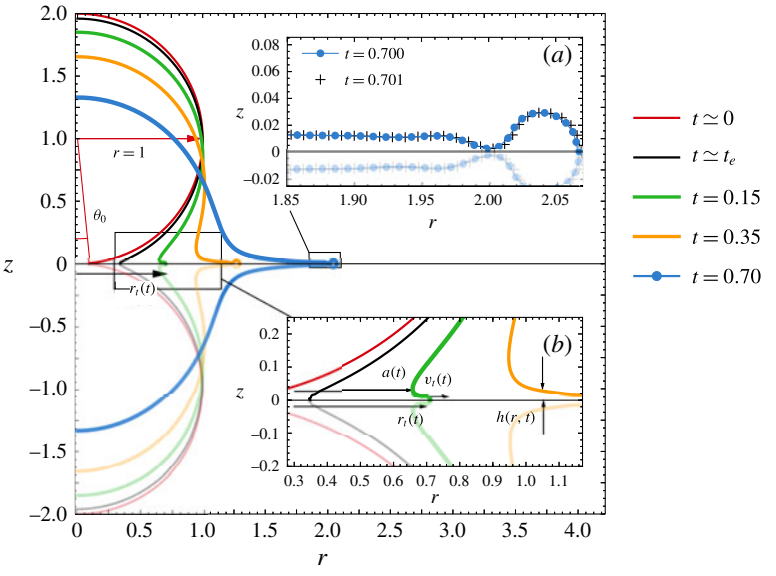


FIGURE 2. (Colour online) The potential flow numerical results start imposing the initial wetted radius, $a = \sin\theta_0 \approx \pi/36$ with $\theta_0 = 5°$. The inset (a) shows the re-gridding procedure used to stabilize the numerical simulation, consisting of placing nodes in between the nodes of the previous time step. The inset (b) is a zoom in of the region from which the lamella is ejected at three different instants of time: t_e, $t = 0.15$ and $t = 0.35$. The figure also illustrates the wetted radius $a(t)$ as well as the radial position of the rim, $r_t(t)$, and its velocity, $v_t(t)$. The inset also shows the definition of height of the lamella, $h(r, t)$, not to be confused with the width of the rim, $h_t(t)$.

in the region near the edge of the lamella, the agreement between experiments and numerical results, is remarkable. The discrepancies in the position of the rim observed in figure 1 are due to the fact that, at room temperature, the viscous shear stresses at the wall contribute to further decelerate the advancing front. We used our own experiments, performed at room temperature, to compare with the numerical results since we could not find in the literature experimental images of drops impacting a hot substrate in the Leidenfrost regime with enough spatio-temporal resolution.

2. Potential flow simulations

Following the notation in RG14, lower case variables will be used in what follows to refer to dimensionless variables, which are constructed here using as scales for velocity, length and pressure V, R and ρV^2, respectively. Since the Froude number $Fr = V^2/gR \gg 1$ and the shear stresses acting on the liquid are negligible, the only relevant dimensionless parameter characterizing the splashing of droplets in the Leidenfrost regime is the Weber number, defined here as $We = \rho V^2 R/\sigma$.

The most relevant event taking place after the impact of a drop in the dynamic Leidenfrost regime is that at t_e, with t_e the ejection time – see figure 2 – an extremely thin liquid sheet of initial thickness $h_t(t_e)$ is expelled tangentially to the substrate with an initial velocity $v_t(t_e)$. In RG14, an algebraic equation for t_e was deduced based on the following facts: (i) prior to the ejection of the lamella, the time evolution of the radius of the wetted area is $a(t) = \sqrt{3t}$ (this result was derived for the very first time

https://doi.org/10.1017/jfm.2016.496 Published online by Cambridge University Press

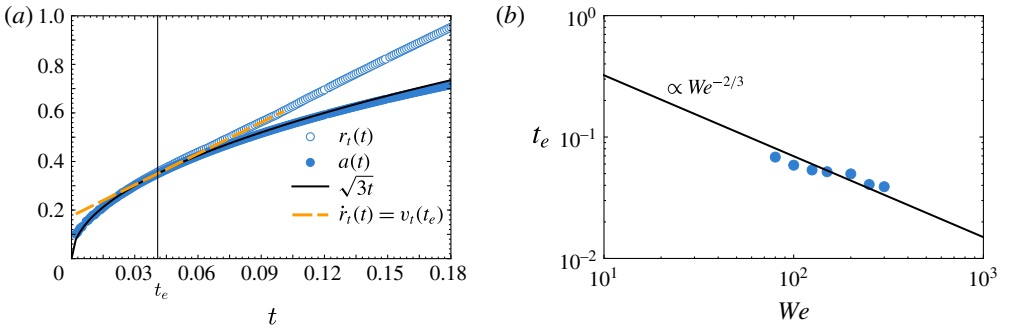


FIGURE 3. (Colour online) (*a*) The figure shows the numerical results for both $a(t)$ and the radial position of the edge lamella $r_t(t)$ in the case of $We = 100$. The vertical line indicates the ejection time predicted by (2.2) and the dashed line represents the predicted position of the rim, ejected from $r = \sqrt{3t_e}$ with an initial velocity $v_t(t_e) = 1/2\sqrt{3/t_e}$, with t_e given in (2.2). (*b*) The ejection times predicted by the BIMs are such that $t_e \propto We^{-2/3}$, in agreement with (2.2).

by Riboux and Gordillo in RG14 using the linearization of the boundary conditions for the potential flow (Wagner 1932)); (ii) at t_e, the velocity of the tip of the lamella is equal to the velocity of the wetted radius, i.e. $v_t(t_e) = \dot{a}(t_e)$ with dots denoting time derivatives; and (iii) the lamella can only be ejected if its tip advances faster than the radius of the wetted area. We concluded in RG14 that t_e can be calculated solving the algebraic equation

$$\frac{\sqrt{3}}{2} Re^{-1} t_e^{-1/2} + We^{-1} = \ddot{a}\, h_t^2 = c^2 t_e^{3/2} \quad \text{with } c = 1.1, \tag{2.1}$$

which expresses the fact that the ejection time is the instant at which the deceleration of the edge of the lamella coincides with the deceleration of the wetted area, $\ddot{a}$. For wall temperatures above T_L, the edge of the lamella is not decelerated by the action of viscous shear stresses and, therefore, setting to infinity the Reynolds number Re in (2.1) yields,

$$t_e = (c^2\, We)^{-2/3}. \tag{2.2}$$

Using the analytical expressions for both $v_t(t_e)$ and $h_t(t_e)$ derived in RG14, as well as the result in (2.2), it can be concluded that $v_t(t_e) = 1/2\sqrt{3/t_e} \propto We^{1/3}$ and $h_t(t_e) = \sqrt{12}\, t_e^{3/2}/\pi \propto We^{-1}$. Figure 3 confirms the result in (2.2), $t_e \propto We^{-2/3}$.

Once the lamella is ejected, as also deduced in RG14, for $t > t_e$ and $t \ll 1$, both the liquid velocity and the height of the liquid layer at $r = a(t) = \sqrt{3t}$, which is the radial position where the drop meets the lamella, are respectively given by $v_a = 2\dot{a} = \sqrt{3/t}$ and $h_a = \sqrt{12}\, t^{3/2}/(3\pi)$. Figure 4 confirm these theoretical predictions for $We \geqslant 100$. More precisely, figure 4 shows that, while the analytical expression for v_a is valid for arbitrary times, the corresponding analytical expression for h_a departs from the numerical results for $t \geqslant 0.1$ (see figure 4*c*). Therefore, the equations describing the liquid velocity in the lamella $u(r, t)$ and its height $h(r, t)$ at $r = \sqrt{3t}$ i.e. at the radial position from which the liquid sheet is ejected for times $t > t_e$, are respectively given

https://doi.org/10.1017/jfm.2016.496 Published online by Cambridge University Press

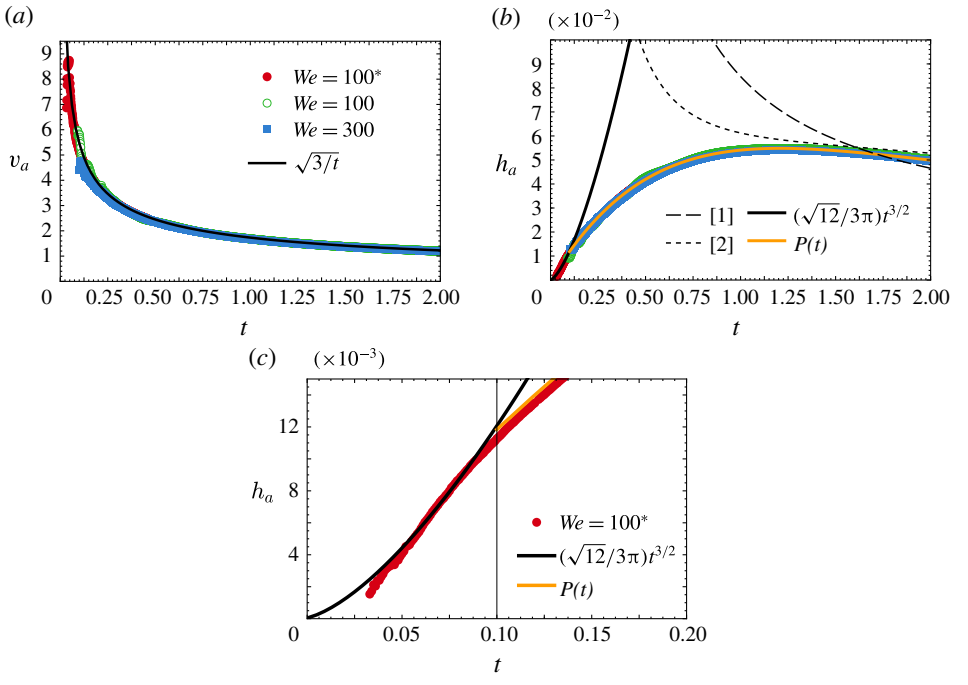


FIGURE 4. (Colour online) (*a*) Comparison between the theoretical expression $v_a = 2\dot{a} = \sqrt{3/t}$ deduced in RG14 and the numerical result. The good agreement between theory and experiments depicted in this figure is independent of the Weber number whenever $We \geqslant 100$. Two of the simulations shown are carried out using $N(T=0) = 501$ whereas in the case marked with an asterisk [*], $N(T=0) = 1001$. (*b*) Comparison of the height of the lamella at $r = \sqrt{3t}$ predicted by the models in Eggers *et al.* (2010) [1] and Roisman (2009) [2] with the numerical result. (*c*) Comparison between the theoretical expression $h_a = h(a(t), t) = (\sqrt{12}/3\pi)\, t^{3/2}$ deduced in RG14, valid for $t \ll 1$ and the numerical result. The vertical line indicates the instant at which we have set the transition between the result predicted by the potential flow theory and the fitting polynomial $P(t)$ in (2.4).

by

$$\left.\begin{aligned} u(r=a,\,t) = v_a = \sqrt{3/t}, \quad & \text{and} \\ h(r=a,\,t) = h_a = \sqrt{12}t^{3/2}/(3\pi) \quad & \text{for } t < 0.1 \\ h(r=a,\,t) = P(t) \quad & \text{for } t \geqslant 0.1, \end{aligned}\right\} \tag{2.3}$$

with

$$\left.\begin{aligned} P(t) = \sum_{i=0}^{5} (0.1p_i)t^i \quad & \text{and} \quad p_0 = -2.453 \times 10^{-3}, \quad p_1 = 1.321, \quad p_2 = -1.176, \\ & p_3 = 0.4943, \quad p_4 = -0.1047, \quad p_5 = 8.89 \times 10^{-3} \end{aligned}\right\} \tag{2.4}$$

a polynomial which is fitted to the numerical results.

The *ad hoc* radial velocity field within the drop proposed by both Roisman (2009) and Eggers *et al.* (2010) is $u(r,\,t) = r/(t+\tau)$, with τ an adjustable order-unity

https://doi.org/10.1017/jfm.2016.496 Published online by Cambridge University Press

constant. While the stagnation point type of flow within the impacting drop hypothesized by Roisman (2009) and Eggers *et al.* (2010) is a good approximation to the real flow field for $t \sim O(1)$, for times such that $t > t_e$, $t \ll 1$, the velocity field at $r \simeq \sqrt{3t}$ does not correspond to a stagnation point flow (see RG14 for details). Interestingly, our theory predicts a radial velocity at $r = a(t) = \sqrt{3t}$, $u(r = a(t), t) = a(t)/t = \sqrt{3/t}$ for $t \ll 1$ which is, by coincidence, the radial velocity corresponding to a stagnation point of flow of the type $u = r/t$ particularized at $r = \sqrt{3t}$. This is why figure 4(*a*) shows a fairly good between the analytical expression $v_a = \sqrt{3/t}$ and the numerical results for arbitrary values of t. Figure 4(*b*) also shows the values of $h_a(t) = h(r = \sqrt{3t}, t)$ predicted by the model in Roisman (2009),

$$h(r, t) = 8\frac{\eta}{(t+\tau)^2}\exp\left[-\frac{6\eta\, r^2}{(t+\tau)^2}\right], \tag{2.5}$$

with $\eta = 0.39$, $\tau = 2 \times 0.25$ and with a constant equal to 8 because here we define dimensionless lengths using the drop radius instead of its diameter, as well as the results predicted by the model in Eggers *et al.* (2010),

$$\left.\begin{aligned} h(r, t) &= \frac{1}{(t+\tau)^2}H(x) \\ H(x) &= \frac{3.19}{(1+Cx^2)^6} \quad \text{with} \quad x(r, t) = \frac{r}{t+\tau}, \end{aligned}\right\} \tag{2.6}$$

with $C = 0.604$ and $\tau = 1$ (Lastakowski *et al.* 2014). Clearly, neither the model by Roisman (2009) not that by Eggers *et al.* (2010) are in agreement with the numerical results.

3. Prediction of the critical Weber number for splashing and of the maximum spreading radius for droplets impacting in the Leidenfrost regime

For a given instant of time $t > t_e$, the lamella extends from the position where the drop meets the liquid sheet i.e. $r = \sqrt{3t}$, down to $r = r_t(t)$, with $r_t(t)$ indicating the radial position of the rim. In RG15, we showed that both the liquid velocity $u(r, t)$ and the height of the liquid layer within the lamella, $h(r, t)$, can be calculated using the pair of equations (Gordillo & Gekle 2010; Villermaux & Bossa 2011),

$$\frac{\mathrm{D}u}{\mathrm{D}t} = 0 \quad \text{and} \quad \frac{\mathrm{D}\ln(rh)}{\mathrm{D}t} = -\frac{\partial u}{\partial r}, \tag{3.1a,b}$$

with $\mathrm{D}/\mathrm{D}t \equiv \partial/\partial t + u\,\partial/\partial r$ the material derivative. The former of the two equations in (3.1*a*,*b*) expresses that fluid particles conserve their velocities within the lamella from $r = \sqrt{3t}$ down to the radial position $r_t(t)$ where the rim is located; the latter is the continuity equation. The pair of equations in (3.1*a*,*b*) representing the ballistic motion of fluid particles along the lamella are solved subject to the initial conditions given in equation (2.3) by means of the Lagrangian numerical method already used in RG15. The results of the model for $h(r, t)$, shown in figure 5, are in excellent agreement with the numerical simulations.

The radial position of the edge of the lamella, $r_t(t)$, as well as its thickness, $h_t(t)$, are deduced by applying the integral balances of mass and momentum at the rim

https://doi.org/10.1017/jfm.2016.496 Published online by Cambridge University Press

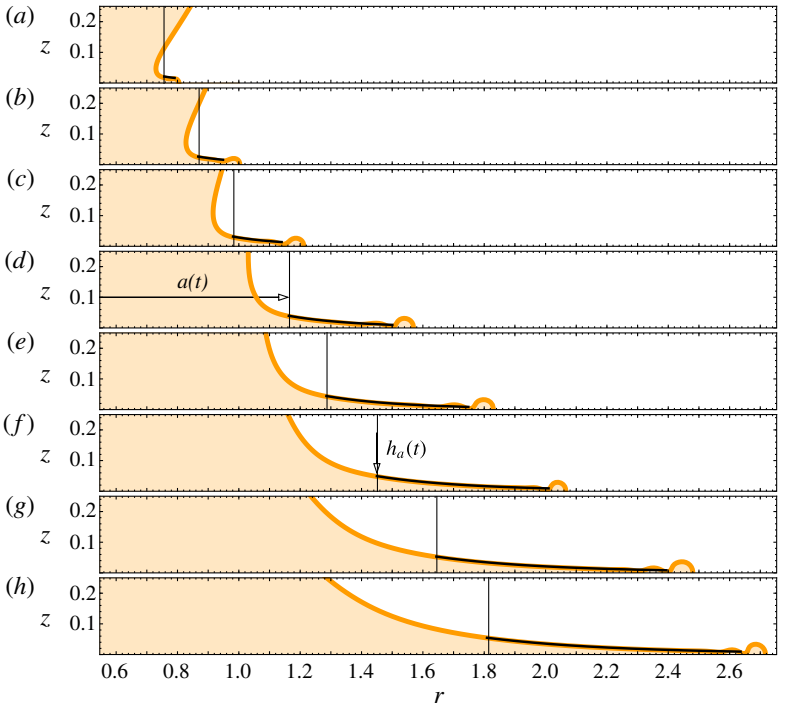


FIGURE 5. (Colour online) Comparison, for $We = 100$, between the height of the lamella predicted by the model – ballistic equations (3.1*a*,*b*) subjected to the boundary conditions given in (2.3) – and the numerical result. The vertical line illustrates the radial position $r = a(t) = \sqrt{3t}$ for several instants of time as well as the height of the lamella at $r = \sqrt{3t}$, $h_a(t) = h(r = \sqrt{3t}, t)$; v_a is the liquid velocity at $r = a(t) = \sqrt{3t}$, namely $v_a = u(r = \sqrt{3t}, t)$. (*a*) $t = 0.19$, (*b*) 0.25, (*c*) 0.32, (*d*) 0.45, (*e*) 0.55, (*f*) 0.70, (*g*) 0.90 and (*h*) $t = 1.10$.

(Taylor 1959; Culick 1960),

$$\left.\begin{aligned} \frac{\mathrm{d}r_t}{\mathrm{d}t} &= v_t, \\ \frac{\pi}{4}\frac{\mathrm{d}h_t^2}{\mathrm{d}t} &= [u(r_t, t) - v_t]h(r_t, t), \\ \frac{\pi\, h_t^2}{4}\frac{\mathrm{d}v_t}{\mathrm{d}t} &= [u(r_t, t) - v_t]^2\, h(r_t, t) - 2\, We^{-1}. \end{aligned}\right\} \tag{3.2}$$

The system of equations (3.2) is solved subjected to the following initial conditions,

$$\left.\begin{aligned} r_t &= a(t_e) = \sqrt{3\, t_e}, \\ v_t &= v_t(t_e) = 1/2\sqrt{3/t_e}, \\ h_t &= h_t(t_e) = \sqrt{12}\, t_e^{3/2}/\pi, \end{aligned}\right\} \tag{3.3}$$

with t_e given by (2.2).

Figure 6(*a*) shows the solution of the system of equations (3.1*a*,*b*)–(3.3) for a particular value of the Weber number, whereas figure 6(*b*) illustrates the comparison

https://doi.org/10.1017/jfm.2016.496 Published online by Cambridge University Press

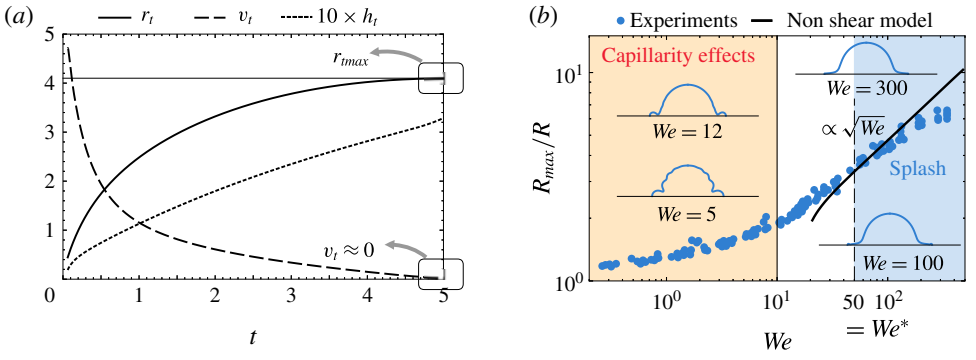


FIGURE 6. (Colour online) (*a*) Radial position r_t, velocity v_t and height h_t of the edge of the lamella as function of the dimensionless time t for $We = 150$. The maximum spreading radius is reached when $r_{t\,max} = R_{max}/R \Longleftrightarrow v_t \approx 0$. (*b*) The predicted maximum spreading radius is of the form $R_{max}/R \propto We^{1/2}$ for $We \gtrsim 20$. The experiments in Tran *et al.* (2012) are plotted for comparison. Two different regimes are observed: for Weber numbers $We \lesssim 10$, capillary waves develop, distorting the initial shape of the drop, whereas for $We > 10$, the impact is dominated by inertia. The black line represents the maximum spreading radius resulting from the self-consistent theory presented here.

between the predicted maximum spreading radius and the experimental data in Tran *et al.* (2012). As was pointed out in Wilderman *et al.* (2016), there are two clearly differentiated regions in the plot r_{max} versus We of figure 6(*b*): the impact is elastic for $We \lesssim 10$ since the initial kinetic energy is transformed into surface energy, as it apparent from the capillary waves developing at the interface of the impacting drop whereas, for $We \gtrsim 10$, the drop spreading process is dominated by inertia. It is discussed in Wilderman *et al.* (2016) that approximately one-half of the initial kinetic energy is dissipated in the sudden expansion connecting the liquid sheet with the rim for $We \geqslant 10$, a fact which is implicitly taken into account in the mass and momentum conservation equations (3.2). In spite of the fact that the system of equations (3.2) is analogous to that used in Roisman (2009), Eggers *et al.* (2010), Villermaux & Bossa (2011) and Lastakowski *et al.* (2014), the crucial difference between the present study and previous ones is that, in our case, we do not impose a specific form for the velocity field within the lamella. Instead, since fluid particles conserve their velocities within the liquid sheet, our system of equations (3.2) subjected to the real initial conditions given in (2.3), with t_e calculated self-consistently through equation (2.2), provides us with the correct expressions for both the liquid velocity $u(r_t)$ and the height of the lamella $h(r_t)$ upstream of the toroidal rim, as can be inferred from the good agreement existing between experiments and predictions depicted in figure 6(*b*).

Another of the advantages of not imposing an *ad hoc* velocity field within the lamella rests in the fact that both the critical Weber number and the diameters and the velocities of the droplets ejected for impact velocities $V > V^*$, which strongly depend on $h(r_t)$, can be calculated self-consistently. Indeed, in RG15, following the ideas in Villermaux & Bossa (2011) and Agbaglah, Josserand & Zaleski (2013), we deduced a criterion for the disintegration of the edge of the liquid sheet based on the fact that the droplets composing the spray result from the amplification in the azimuthal direction of Rayleigh–Taylor and capillary instabilities. The growth rates of the disturbances developing in the azimuthal direction of the toroidal rim are highly attenuated as

https://doi.org/10.1017/jfm.2016.496 Published online by Cambridge University Press

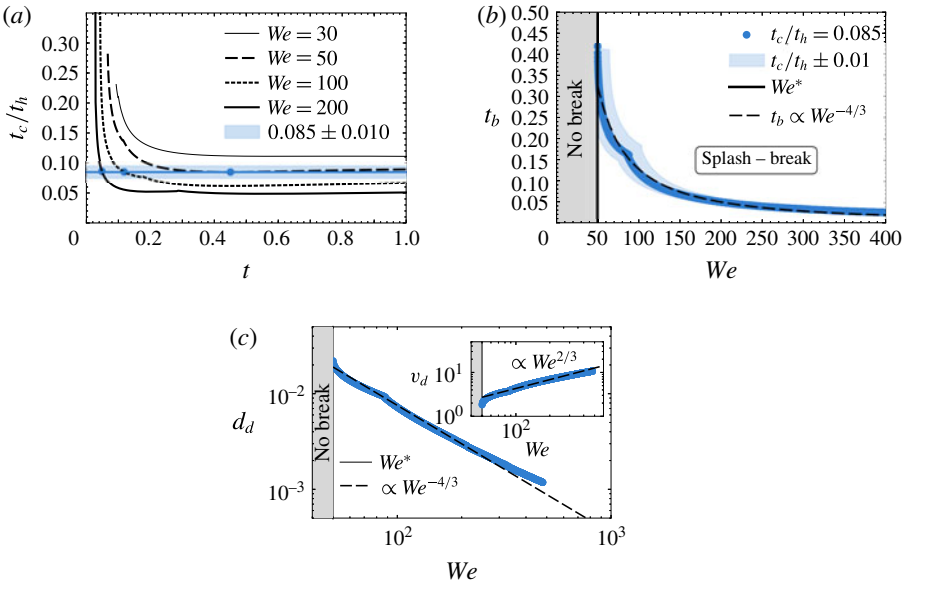


FIGURE 7. (Colour online) (*a*) Ratio t_c/t_h as function of t for several values of the Weber number. The theory in RG15 predicts the disintegration of the toroidal rim when $0.075 \leqslant t_c/t_h \leqslant 0.095$ (area coloured in blue). Therefore, the predicted critical Weber number is $We^* \simeq 50$. (*b*) For $We > We^*$, the rim breaks at $t_b \propto We^{-4/3}$. (*c*) The diameters and velocities of the droplets ejected for $We > We^*$ calculated numerically are approximated here as $d_d = h_t(t_b) \propto We^{-4/3}$ and $v_d = v_t(t_b) \propto We^{2/3}$ respectively.

a consequence of the simultaneous growth of its thickness. In consequence, we concluded that drops will only be ejected when the time characterizing the radial growth of the rim, $T_h = (R/V)t_h = (1/H_t\,\mathrm{d}H_t/\mathrm{d}T)^{-1}$, is substantially larger than the capillary time $T_c = (R/V)t_c = (\rho H_t^3/8\sigma)^{1/2}$. The breakup time t_b is fixed at the instant at which $t_c/t_h \simeq 0.085$ for the reasons explained in RG15, which are reproduced here for the sake of clarity: (i) the characteristic time of growth of a capillary instability is $\sim 3\,T_c$, (ii) a Rayleigh's stability analysis of capillary perturbations reveals that the dimensionless wavenumber k with a fastest growth rate is $k = \pi H_t/\lambda \simeq 0.7$, where λ indicates the wavelength of the perturbation, which is kept constant in time and (iii) the growth of capillary instabilities is inhibited for $k \geqslant 1$ (Eggers & Villermaux 2008). Therefore, in order for capillary corrugations with characteristic initial wavenumbers $k = 0.7$ to be amplified up to the point that drops are ejected from the rim, it is necessary that, in a time $3\,T_c$, $\Delta k < 0.3$ or, equivalently, that $(\mathrm{d}H_t/\mathrm{d}T) \times 3T_c \lesssim 0.3H_t \Rightarrow T_c/T_h \lesssim 0.1$, a value which is very close to $t_c/t_h \simeq 0.085$.

It is depicted in figure 7(*a*) that the ratio t_c/t_h is above the threshold 0.085 for $We \lesssim 50$, a fact meaning that the drop never splashes for values of the Weber number, based on R, below 50. Therefore, the critical Weber number predicted by our approach is $We^* = 50$, a value which is rather close to the experimental one reported in Staat *et al.* (2015), who find that We^* based on R slightly varies with temperature within the range $We^* \simeq 55$–100. Let us point out that We^* is insensitive to the specific value chosen for the threshold t_c/t_h, whenever this value is included within the range $0.075 \leqslant t_c/t_h \leqslant 0.095$ (see the shaded region in figure 7). For values of the Weber number above the critical, figure 7(*b*) shows that the dimensionless breakup time

https://doi.org/10.1017/jfm.2016.496 Published online by Cambridge University Press

decreases with We as $t_b \propto We^{-3/4}$ and, motivated by the good agreement existing between experiments and theory reported in RG15, the diameters and the velocities of the tiny droplets ejected radially outwards from the toroidal rim are calculated respectively as $d_d = h_t(t_b)$ and $v_d = v_t(t_b)$. The numerical values for both $d_d \propto We^{-4/3}$ and $v_d \propto We^{2/3}$, which need experimental validation, are provided in figure 7(*c*).

4. Conclusions

In this contribution we have developed a self-consistent theory to predict the critical Weber number for splashing, We^*, when droplets impact against a solid substrate heated above the dynamic Leidenfrost temperature, T_L (Tran *et al.* 2012, 2013). Our theory is based on the fact that, in the dynamic Leidenfrost regime, the viscous shear stresses acting on the bottom of the drop can be neglected thanks to the vapour layer preventing the liquid drop from touching the substrate. Therefore, the velocity field within the lamella, which is ejected radially outwards and tangentially to the substrate from $r = \sqrt{3t}$ for times after impact $t > t_e$, with t_e the ejection time, can thus be described by means of a ballistic approach. In contrast with previous studies (Roisman 2009; Eggers *et al.* 2010; Villermaux & Bossa 2011) we do not impose a specific form for the velocity field within the lamella. Instead, since fluid particles conserve their velocities within the liquid sheet, we impose as boundary conditions for the ballistic equations describing the flow in the lamella the numerical results obtained using a BIM code. These boundary conditions agree well with the expressions deduced in RG14 in the limit $t \ll 1$. Once the flow in the lamella is calculated, both the position and the diameter of the edge of the liquid sheet are determined using integral balances of mass and momentum (Taylor 1959; Culick 1960). The maximum spreading radius of drops impacting in the dynamic Leidenfrost regime are then calculated in a self-consistent manner, and the results obtained are in good agreement with the experimental data provided in Tran *et al.* (2012). Making use of the fact that drops will only be ejected from the rim when the time characterizing the radial growth of the edge of the lamella is substantially larger than the capillary time, we conclude that $We^* \simeq 50$. This value is also in good agreement with the experimental values reported in Staat *et al.* (2015). For $We > We^*$, using the approach described in RG15, we also provide closed expressions for the diameters and for the velocities of the droplets composing the spray as a function of the Weber number. These expressions need experimental validation.

Acknowledgements

This study has been financially supported by the Spanish MINECO under Project DPI2014-59292-C3-2-P, partly financed through European funds.

REFERENCES

AGBAGLAH, G., JOSSERAND, C. & ZALESKI, S. 2013 Longitudinal instability of a liquid rim. *Phys. Fluids* **25**, 022103.

CULICK, F. E. C. 1960 Comments on a ruptured soap film. *J. Appl. Phys.* **31** (1274), 1128–1129.

DUEZ, C., YBERT, C., CLANET, C. & BOCQUET, L. 2007 Making a splash with water repellency. *Nat. Phys.* **3**, 180–183.

EGGERS, J., FONTELOS, M. A., JOSSERAND, C. & ZALESKI, S. 2010 Drop dynamics after impact on a solid wall: theory and simulations. *Phys. Fluids* **22** (6), 062101.

https://doi.org/10.1017/jfm.2016.496 Published online by Cambridge University Press

EGGERS, J. & VILLERMAUX, E. 2008 Physics of liquid jets. *Rep. Prog. Phys.* **71**, 036601.

GORDILLO, J. M. & GEKLE, S. 2010 Generation and breakup of worthington jets after cavity collapse. Part 2. Tip breakup of stretched jets. *J. Fluid Mech.* **663**, 193–330.

JOSSERAND, C. & THORODDSEN, S. T. 2016 Drop impact on a solid surface. *Annu. Rev. Fluid Mech.* **48**, 365–391.

LASTAKOWSKI, H., BOYER, F., BIANCE, A.-L., PIRAT, C. & YBERT, C. 2014 Bridging local to global dynamics of drop impact onto solid substrates. *J. Fluid Mech.* **747**, 103–118.

RIBOUX, G. & GORDILLO, J. M. 2014 Experiments of drops impacting a smooth solid surface: a model of the critical impact speed for drop splashing. *Phys. Rev. Lett.* **113**, 024507.

RIBOUX, G. & GORDILLO, J. M. 2015 The diameters and velocities of the droplets ejected after splashing. *J. Fluid Mech.* **772**, 630–648.

RODRÍGUEZ–RODRÍGUEZ, J., GORDILLO, J. M. & MARTÍNEZ–BAZÁN, C. 2006 Breakup time and morphology of drops and bubbles in a high-Reynolds-number flow. *J. Fluid Mech.* **548**, 69–86.

ROISMAN, I. V. 2009 Inertia dominated drop collisions. Part II. An analytical solution of the Navier–Stokes equations for a spreading viscous film. *Phys. Fluids* **21**, 052104.

SHIROTA, M., VAN LIMBEEK, M. J., SUN, C., PROSPERETTI, A. & LOHSE, D. 2016 Dynamic Leidenfrost effect: relevant time- and length-scales. *Phys. Rev. Lett.* **116**, 064501.

STAAT, H. J. J., TRAN, T., GEERDINK, B., RIBOUX, G., SUN, C., GORDILLO, J. M. & LOHSE, D. 2015 Phase diagram for droplet impact on superheated surfaces. *J. Fluid Mech.* **779** (R3), 1–12.

TAYLOR, G. I. 1959 The dynamics of thin sheets of fluid. Part II. Waves on fluid sheets. *Proc. R. Soc. Lond.* A **253** (1274), 296–312.

TRAN, T., STAAT, H. J. J., SUSARREY–ARCE, A., FOERTSCH, T. C., VAN HOUSELT, A., GARDENIERS, H. J. G. E., PROSPERETTI, A., LOHSE, D. & SUN, C. 2013 Droplet impact on superheated micro-structured surfaces. *Soft Matt.* **9**, 3272–3282.

TRAN, T., STAAT, H. J. J., PROSPERETTI, A., SUN, C. & LOHSE, D. 2012 Drop impact on superheated surfaces. *Phys. Rev. Lett.* **108**, 036101.

VILLERMAUX, E. & BOSSA, B. 2011 Drop fragmentation on impact. *J. Fluid Mech.* **668**, 412–435.

WAGNER, H. 1932 Phenomena associated with impacts and sliding on liquid surfaces. *Z. Angew. Math. Mech.* **12**, 193–215.

WILDERMAN, H., VISSER, C. W., SUN, C. & LOHSE, D. 2016 On the spreading of impacting drops. *J. Fluid Mech.* (submitted) arXiv:1602.03782.

XU, L., ZHANG, W. W & NAGEL, S. R. 2005 Drop splashing on a dry smooth surface. *Phys. Rev. Lett.* **94**, 184505.

https://doi.org/10.1017/jfm.2016.496 Published online by Cambridge University Press